

RESEARCH ARTICLE

PET/MRI and PET/CT Radiomics in Primary Cervical Cancer: A Pilot Study on the Correlation of Pelvic PET, MRI, and CT Derived Image Features

Shadi A. Esfahani^{1,2}, Angel Torrado-Carvajal^{2,3}, Barbara Juarez Amorim⁴, David Groshar^{5,6}, Liran Domachevsky^{5,6}, Hanna Bernstine^{5,6}, Dan Stein⁶, Debra Gervais¹, and Onofrio A. Catalano^{1,2}

¹Department of Radiology, Division of Abdominal Imaging, Massachusetts General Hospital and Harvard Medical School, Boston, MA, USA

²Athinoula A. Martinos Center for Biomedical Imaging, Department of Radiology, Massachusetts General Hospital Boston and Harvard Medical School, Boston, MA, USA

³Medical Image Analysis and Biometry Lab, Universidad Rey Juan Carlos, Madrid, Spain

⁴Division of Nuclear Medicine, State University of Campinas (UNICAMP), Campinas, Brazil

⁵Sackler School of Medicine, Tel-Aviv University, Tel-Aviv, Israel

⁶Department of Nuclear Medicine and Radiology, Assuta Medical Centers, Tel-Aviv, Israel 2021

Abstract

Purpose: To evaluate the correlation of radiomic features in pelvic [2-deoxy-2-¹⁸F]fluoro-D-glucose positron emission tomography/magnetic resonance imaging and computed tomography ([¹⁸F]FDG PET/MRI and [¹⁸F]FDG PET/CT) in patients with primary cervical cancer (CCa).

Procedures: Nineteen patients with histologically confirmed primary squamous cell carcinoma of the cervix underwent same-day [¹⁸F]FDG PET/MRI and PET/CT. Two nuclear medicine physicians performed a consensus reading in random order. Free-hand regions of interest covering the primary cervical tumors were drawn on PET, contrast-enhanced pelvic CT, and pelvic MR (T2 weighted and ADC) images. Several basic imaging features, standard uptake values (SUV_{mean}, SUV_{max}, and SUV_{peak}), total lesion glycolysis (TLG), metabolic tumor volume (MTV), and more advanced texture analysis features were calculated. Pearson's correlation test was used to assess the correlation between each pair of features. Features were compared between local and metastatic tumors, and their role in predicting metastasis was evaluated by receiver operating characteristic curves.

Results: For a total of 101 extracted features, 1104/5050 pairs of features showed a significant correlation ($\rho \geq 0.70$, $p < 0.05$). There was a strong correlation between 190/484 PET pairs of features from PET/MRI and PET/CT, 91/418 pairs of CT and PET from PET/CT, 79/418 pairs of T2 and PET from PET/MRI, and 50/418 pairs of ADC and PET from PET/MRI. Significant difference was seen between eight features in local and metastatic tumors including MTV, TLG, and entropy on PET from PET/CT; MTV and TLG on PET from PET/MRI; compactness and entropy on T2; and entropy on ADC images.

Conclusions: We demonstrated strong correlation of many extracted radiomic features between PET/MRI and PET/CT. Eight radiomic features calculated on PET/CT and PET/MRI were significantly different between local and metastatic CCa. This study paves the way for future studies to evaluate the diagnostic and predictive potential of radiomics that could guide clinicians toward personalized patients care.

Shadi A. Esfahani and Angel Torrado-Carvajal contributed equally to this manuscript.

Correspondence to: Onofrio A. Catalano; e-mail: ocatalano@mgh.harvard.edu

Key words PET/CT · PET/MRI · PET/MR · Cervical cancer · Squamous cell carcinoma · Radiomics · [2-deoxy-2-¹⁸F]fluoro-D-glucose

INTRODUCTION

Cervical cancer (CCa) is the fourth most commonly diagnosed cancer and the fourth leading cause of cancer death in women worldwide [1]. The overall recurrence and survival of CCa mainly depends on early diagnosis, precise delineation of the primary tumor, and detection of potential metastases during the initial diagnostic workup [2, 3]. Hence, accurate initial staging and biological characterization of CCa is crucial to provide the best possible clinical management and predict prognosis and response to treatment [3, 4]. Over the past decade, 2-deoxy-2-[¹⁸F]fluoro-D-glucose positron emission tomography/computed tomography ([¹⁸F]FDG PET/CT) has been widely used for tumor detection and monitoring treatment response in clinical practice by providing information about the metabolic activity of the tumors in addition to the anatomical details [4–6]. However, given the radiation exposure risks and suboptimal soft tissue resolution of CT, development of an integrated imaging tool for optimal imaging of CCa is of utmost clinical need. MRI has been established as a valuable imaging modality for the assessment of local extent and potential metastatic lesions in CCa [7]. Aside from morphologic imaging, the imaging biomarkers derived from diffusion weighted imaging (DWI) and apparent diffusion coefficient (ADC) have been studied in gynecologic oncological imaging [8]. Recent introduction of integrated PET/MRI systems has provided the basis for acquisition and correlation of simultaneously derived morphologic and metabolic data, which could potentially result in a reduction of co-registration and motion artifacts in addition to elimination of ionizing radiation risks from the CT component of hybrid imaging [8–11].

In addition, introduction of radiomics has opened new avenues for better understanding of the underlying biology of the tumors at high risk for local invasion, metastases, and recurrence [4, 12]. Radiomics uses data-characterization algorithms to extract large amounts of quantitative features, potentially uncovering characteristics that may be invisible to our naked eye [13] and helping the radiologists with providing more data on the tumors biological behavior [7]. Multiple previous studies have identified a potential relationship between advanced radiomic features derived from [¹⁸F]FDG PET, CT, and MR images and clinicopathological characteristics of many types of tumors, suggesting that their combination can improve characterization of tumor microenvironment and the accuracy of predicting the clinical behavior of neoplastic diseases [4, 14, 15]. However, similar research in CCa,

particularly the primary cervical squamous cell carcinoma (SCC), is limited, and such relationship between hybrid pelvic [¹⁸F]FDG PET/CT and [¹⁸F]FDG PET/MRI advanced features is not well established [16]. In addition, the use of radiomics in predicting CCa regional lymphadenopathy and distant metastases is not yet clear and needs to be further investigated.

In the present paper, we evaluated the potential correlation of multiple imaging features in pelvic PET, ADC, and T2 weighted images of hybrid [¹⁸F]FDG PET/MRI, and the features of pelvic PET and CT images of hybrid [¹⁸F]FDG PET/CT in patients with primary CCa. To this end, we computed multiple radiomic features from different imaging modalities and studied the consistency of data between [¹⁸F]FDG PET/MRI and [¹⁸F]FDG PET/CT, as well as the correlation between different imaging features. In the next step, we explored whether these imaging features vary between locally confined and metastatic tumors.

MATERIALS AND METHODS

Patient Population

In this institutional review board–approved retrospective study, 19 patients with histologically proven squamous cell carcinoma (SCC) of the cervix who underwent same-day [¹⁸F]FDG PET/CT and [¹⁸F]FDG PET/MRI for primary tumor staging between September 2017 and January 2019 were evaluated. The inclusion criteria were defined as confirmed diagnosis of CCa on biopsy; no prior surgical, chemotherapy, or radiation therapy; and available [¹⁸F]FDG PET/MRI and [¹⁸F]FDG PET/CT data on initial diagnostic workup. The exclusion criteria included any type of prior treatment of the primary CCa, tumor types other than SCC, blood glucose level of more than 140 mg/dl, PET acquisition interval longer than 100 min after intravenous [¹⁸F]FDG injection, and small tumors not detectable on PET.

[¹⁸F]FDG PET/MRI and [¹⁸F]FDG PET/CT Acquisition

Patients fasted for at least 6 h before the imaging studies and peripheral blood glucose was measured immediately before [¹⁸F]FDG administration to ensure its level was less than 140 mg/dl. Whole-body PET/CT and venous phase contrast-enhanced diagnostic CT images were acquired from the base of the skull to mid thighs approximately 60 min after intravenous injection of 344 ± 68 MBq (mean \pm SD) [¹⁸F]FDG. Immediately after the PET/CT acquisition, patients underwent PET/MRI, approximately 80–100 min after [¹⁸F]FDG injection. PET and MRI data (T2 weighted, DWI and ADC maps) including the dedicated high-resolution T2 weighted sequences of the cervix, reported in Supplemental Table 1, were acquired simultaneously on a Siemens Biograph mMR scanner (Siemens Healthineers, Erlangen, Germany) accordingly to previously described scanning protocols [17, 18].

Simultaneous PET acquisition lasted the entire MRI acquisition, 12 ± 2.5 min (range 9.6–17.1 min).

Image Analysis and Feature Extraction

Using Horos software (version 4, LGPL 4.0), two nuclear medicine physicians/radiologists with 5 and 12 years of expertise in acquiring and interpreting PET/MRI manually delineated regions of interest (ROIs), in consensus, over the entire primary tumors. The ROIs were delimited separately on PET of PET/CT, CT, PET of PET/MRI, and T2 weighted and ADC images on the axial slices of each image set. An example of the ROI delineation on axial images is shown in Fig. 1.

Using the feature extraction package QTIM Tools (Quantitative Translational Imaging in Medicine Lab, Athinoula A. Martinos Center for Biomedical Imaging, Boston, MA, USA) [9], 95 image features were extracted from all 5 image sets (PET from ^{18}F]FDG PET/CT, CT, PET from ^{18}F]FDG PET/MRI, T2, and ADC). Shape features (total of eight for each image set) included voxel count, volume (mm^3), surface area (mm^2), volume–surface area ratio, compactness, compactness alternate, spherical disproportion, and sphericity. Intensity features (total of 11 for each image set) included standard distribution statistics such as mean, minimum (min), maximum (max), median, range, SD, variance, entropy, kurtosis, skewness, and covariance. In addition, for ^{18}F]FDG PET images, the SUV_{peak} (defined as the mean SUV value in a 1-cm^3 sphere centered in the SUV_{max} value), metabolic tumor volume (MTV), and total lesion glycolysis (TLG) were calculated using methods previously described [9, 19]. The computation of all these features resulted in a total of 101 extracted radiomic features.

Statistical Analysis

Statistical analysis was performed using Matlab (The MathWorks Inc., Natick, MA, USA) and GraphPad Prism 9.0 (GraphPad Software Inc., San Diego, CA, USA). Pairwise Pearson’s linear correlation coefficients were computed among each pair of radiomic features. Correlation and regression analyses were run to assess the radiomic features in intra-modality and inter-modality scenarios. Correlation analyses results are shown as number of significantly correlated features (with $\rho \geq 0.70$ and $p < 0.05$)/total number of features which include all of the possible pairs of correlations in that specific analysis obtained after excluding symmetrical duplicates and autocorrelations in the intra-modality scenarios. A linear regression model was fit between those features showing a high correlation between modalities. The most clinically valuable linear regression models including estimated coefficient, intercept, and adjusted R^2 and p values were calculated. Comparison of difference between the mean values of image features in local and metastatic tumor groups was performed using unpaired Wilcoxon rank test. Statistical

significance was considered when the p value was lower than 0.05. Receiver operating characteristic (ROC) curves with the CI of 95 % were generated to determine a cutoff for the imaging features that were significantly different between the local and metastatic tumors.

RESULTS

Patients

The imaging data for a total of 19 patients with CCa who underwent ^{18}F]FDG PET/CT and ^{18}F]FDG PET/MRI were evaluated. Five patients were excluded due to the following reasons: long ^{18}F]FDG injection–PET imaging interval being more than 100 min in two patients, small size of the tumor (less than 1 cm^3 and not detectable on PET images) in one patient, and motion degraded images in two patients. Images of 14 patients met the criteria for data analysis. Patients were staged according to both the International Federation of Gynecology and Obstetrics (FIGO) staging system [20] and the 8th version of the TNM staging system by the American Joint Committee on Cancer [21]. According to FIGO staging, patients were classified into two groups of SCC: (1) local disease (4 patients with stage IB and 3 with stage IIB, $n = 7$); (2) metastatic disease (stage IVB, $n = 7$). According to TNM staging, patients were classified into two major groups of SCC: (1) without nodal spread of the tumor (N0M0, $n = 7$); (2) with nodal spread of disease (N1M1, $n = 7$). Patients’ detailed TNM and FIGO staging is demonstrated in Table 1.

Radiomic Features Correlation and Regression Analysis

The correlogram corresponding to the cross-correlation matrix for all of 101 extracted radiomic features is shown on

Table 1. Patients’ cervical cancer characteristics based on TNM and FIGO staging

Subject ($n = 14$)	TNM stage	FIGO stage
1	T2bN1M1	4B
2	T2bN1M1	4B
3	T1N1M1	4B
4	T2bN1M1	4B
5	T2bN1M1	4B
6	T2bN1M1	4B
7	T2bN1M1	4B
8	T2bN0M0	2B
9	T1N0M0	1B1
10	T1N0M0	1B1
11	T1N0M0	1B2
12	T1N0M0	1B1
13	T2bN0M0	2B
14	T2AN0M0	2B

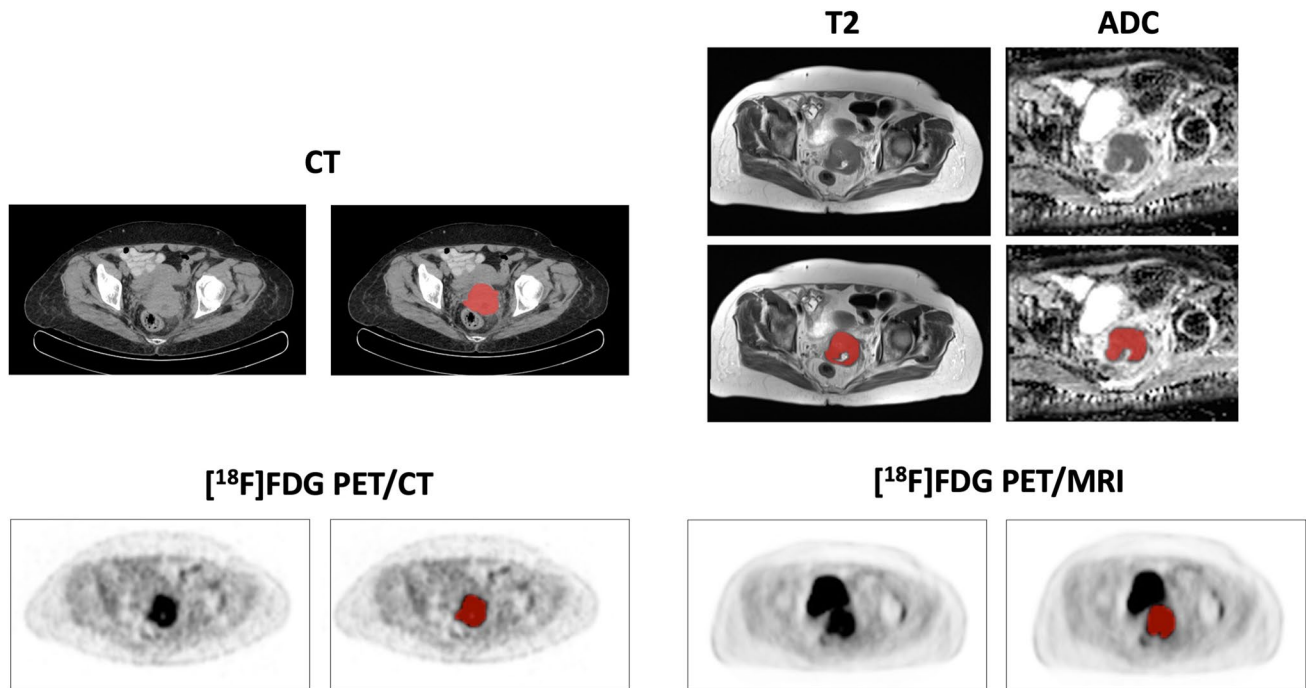


Fig. 1. Representative axial images of contrast enhanced CT, $[^{18}\text{F}]$ FDG PET/CT, T2 weighted, apparent diffusion coefficient (ADC), and $[^{18}\text{F}]$ FDG PET/MRI of the pelvis and regions of interests (in red) for evaluation of radiomic features of the primary cervical squamous cell carcinoma.

Fig. 2. From total of unique 5050 correlations between pairs of radiomic features (obtained after excluding symmetrical duplicates and autocorrelations from 10,201 correlation pairs in the cross-correlation matrix), a total of 1104 pairs of features showed a strong correlation ($\rho \geq 0.70$, $p < 0.05$). Many pairs of features from the same modality demonstrated a high correlation (strongly correlated pairs of features on PET from PET/CT = 101/231, CT = 34/171, PET from PET/MRI = 86/231, T2 = 35/171, and ADC = 37/171, $\rho \geq 0.70$, $p < 0.05$). In addition, a strong correlation was observed between 190/484 pairs of PET features from PET/CT and PET/MRI. In the present study, we focused our subsequent analyses on the correlation of features between different modalities to further investigate the potential complementary role of radiomic features in multimodal imaging. As such, significantly strong correlation was found between 91/418 pairs of features on PET from PET/CT and CT, 79/418 pairs of features on PET from PET/MRI and T2, and 50/418 pairs of features on PET from PET/MRI and ADC images.

Correlation of Radiomic Features on PET from $[^{18}\text{F}]$ FDG PET/CT and PET from $[^{18}\text{F}]$ FDG PET/MRI

A strong correlation was observed between all of the corresponding (same feature calculated on both modalities) image features on PET from PET/CT and PET from PET/MRI (19/22 pairs of features, $\rho \geq 0.70$, $p < 0.001$) with an exception for SUV_{\min} , $\text{SUV}_{\text{skewness}}$, and $\text{SUV}_{\text{curtosis}}$. Fig. 3 demonstrates representative fitted linear regression models

between the SUV_{mean} of PET from PET/CT and SUV_{mean} of PET from PET/MRI ($\rho = 0.85$, $p < 0.001$), and between the TLG derived from PET of PET/CT and TLG derived from PET of PET/MRI ($\rho = 0.98$, $p < 0.001$), highlighting a strong direct correlation between PET features on PET/CT and PET/MRI.

Correlation of Radiomic Features on CT and PET from $[^{18}\text{F}]$ FDG PET/CT

A strong correlation was found between 91 out of 418 pairs of features on CT and PET from PET/CT (91/418 pairs of features, $\rho \geq 0.70$, $p < 0.001$); of these, we chose 17 pairs with more clinical relevance as shown in Table 2. As expected, the anatomical (CT) and metabolic (PET) volumes were highly correlated ($\rho = 0.8$, $p < 0.001$). The PET metabolic features demonstrated a significant positive correlation with CT_{max} ($\rho = 0.6-0.7$, $p < 0.05$) and $\text{CT}_{\text{compactness}}$ ($\rho = 0.7-0.8$, $p < 0.01$), and a significant inverse correlation with $\text{CT}_{\text{entropy}}$ ($\rho = -0.6$ to -0.8 , $p < 0.05$). In addition, there was a strong inverse correlation between the $\text{PET}_{\text{entropy}}$ and $\text{CT}_{\text{compactness}}$ ($\rho = -0.77$, $p < 0.001$) and between the PET_{MTV} and $\text{CT}_{\text{entropy}}$ ($\rho = -0.57$, $p < 0.05$) (Table 2).

Correlation of Radiomic Features on T2 Weighted and PET Images from $[^{18}\text{F}]$ FDG PET/MRI.

A total of 79 out of 418 pairs of features on T2 and PET from PET/MRI demonstrated a strong correlation (79/418 pairs of

Pearson Correlation Coefficient Between Features

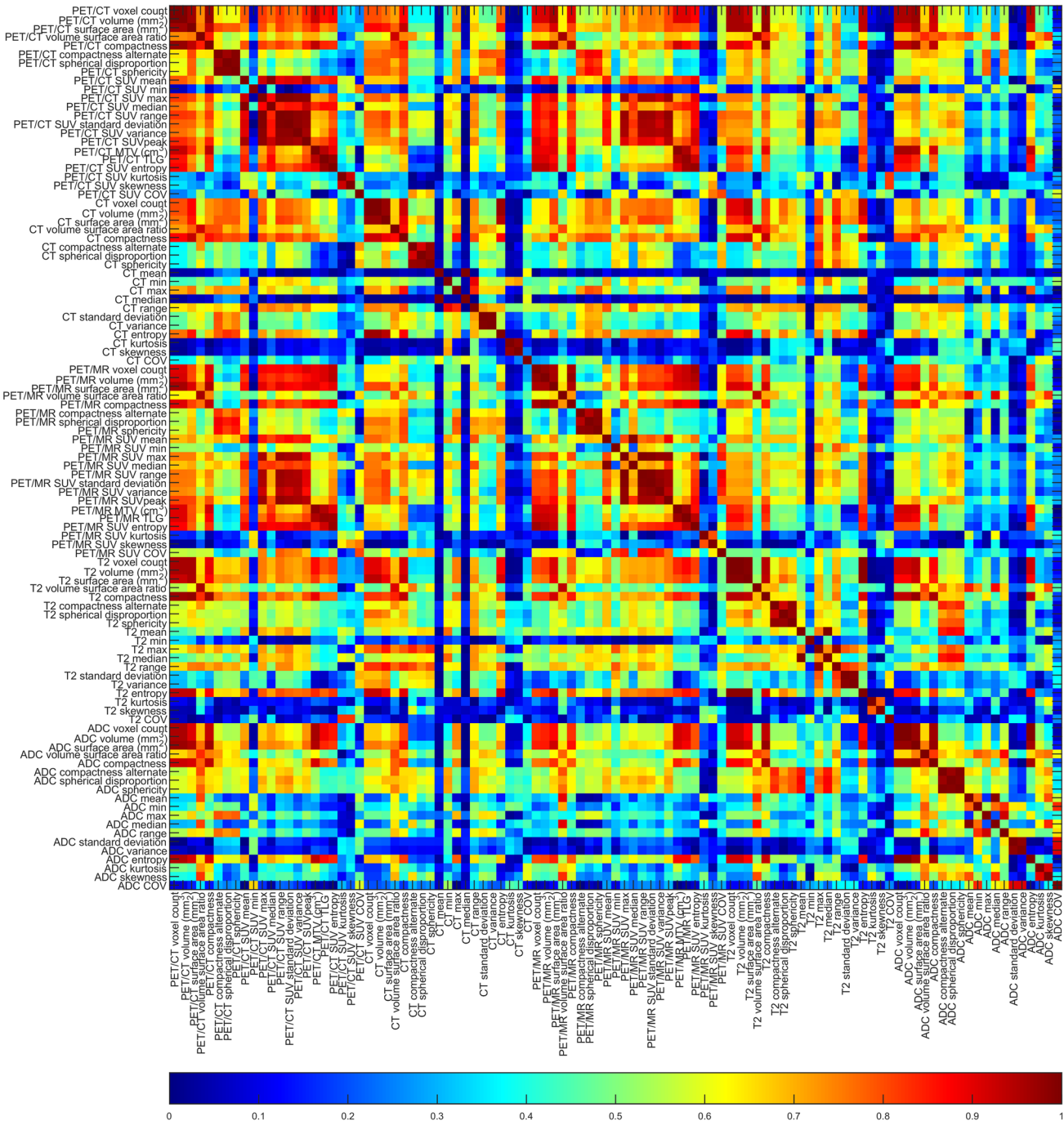


Fig. 2. Correlation matrix showing Pearson's correlation coefficient for all image-derived features. A high correlation was shown between many PET from PET/CT and PET/MRI anatomic and metabolic features. Several features from the same modality demonstrated a high correlation, particularly on PET. In addition, there was a strong correlation between many imaging features of different modalities including between PET/MRI and T2w, PET from PET/MRI and ADC, and PET/CT and CT.

features, $\rho \geq 0.70$, $p < 0.001$), from which 16 more clinically relevant features have been depicted in Table 3. This includes a significant positive correlation between T2_{compactness} and

SUV_{peak} and MTV and TLG on PET ($\rho > 0.78$, $p < 0.001$), and a significant negative correlation of T2_{sphericity} and

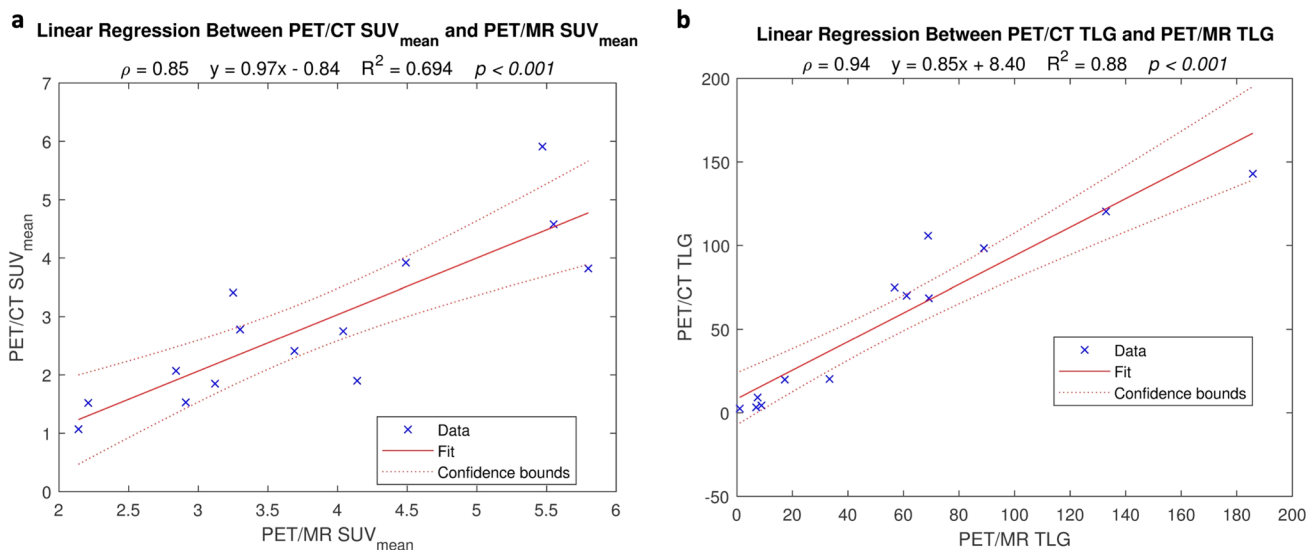


Fig. 3. Representative linear regression models demonstrating strong positive correlation between SUV_{mean} values on PET/CT and PET/MRI (a) and TLG values on PET/CT and PET/MRI (b).

Table 2. Pearson correlation coefficients and associated p values between selected [^{18}F]FDG PET/CT and CT radiomic features in primary cervical cancer

PET/CT feature	CT feature	Pearson correlation (ρ)	p value
Volume	Volume	0.8	<0.01
SUV_{mean}	CT_{max}	0.7	<0.05
SUV_{max}	CT_{max}	0.6	<0.05
SUV_{peak}	CT_{max}	0.67	<0.05
MTV	CT_{max}	0.7	<0.05
TLG	CT_{max}	0.6	<0.05
SUV_{mean}	$CT_{compactness}$	0.8	<0.01
SUV_{max}	$CT_{compactness}$	0.8	<0.01
SUV_{peak}	$CT_{compactness}$	0.8	<0.01
MTV	$CT_{compactness}$	0.8	<0.01
TLG	$CT_{compactness}$	0.7	<0.05
Entropy	$CT_{compactness}$	-0.7	<0.05
Sphericity	$CT_{entropy}$	0.8	<0.05
SUV_{mean}	$CT_{entropy}$	-0.6	<0.05
SUV_{max}	$CT_{entropy}$	-0.7	<0.01
SUV_{peak}	$CT_{entropy}$	-0.7	<0.05
MTV	$CT_{entropy}$	-0.6	<0.05

$T2_{entropy}$ with multiple PET metabolic features, as detailed in Table 3.

Correlation of Radiomic Features on ADC and PET from [^{18}F] FDG PET/MRI.

Fifty out of 418 pairs of features on ADC and PET from PET/MRI demonstrated significant correlation (50/418 pairs of features, $\rho \geq 0.70$, $p < 0.001$). While multiple features including $ADC_{sphericity}$, $ADC_{entropy}$, and $ADC_{curtosis}$ demonstrated a

Table 3. Pearson correlation coefficients and associated p values between selected [^{18}F]FDG PET/MRI and T2 image-derived radiomic features in primary cervical cancer

PET/MRI feature	T2 feature	Pearson correlation (ρ)	p value
Volume	Volume	0.8	<0.01
SUV_{peak}	$T2_{compactness}$	0.78	<0.01
MTV	$T2_{compactness}$	0.85	<0.01
TLG	$T2_{compactness}$	0.83	<0.01
SUV_{mean}	$T2_{sphericity}$	-0.68	<0.05
SUV_{max}	$T2_{sphericity}$	-0.56	<0.05
SUV_{peak}	$T2_{sphericity}$	-0.6	<0.05
SUV_{mean}	$T2_{mean}$	0.64	<0.05
SUV_{max}	$T2_{mean}$	0.67	<0.05
SUV_{peak}	$T2_{mean}$	0.66	<0.05
Sphericity	$T2_{entropy}$	0.62	<0.05
SUV_{mean}	$T2_{entropy}$	-0.74	<0.01
SUV_{max}	$T2_{entropy}$	-0.75	<0.01
SUV_{peak}	$T2_{entropy}$	-0.8	<0.01
MTV	$T2_{entropy}$	-0.82	<0.01
TLG	$T2_{entropy}$	-0.86	<0.01

significant inverse correlation with the metabolic features of PET (Table 4), no significant correlation was found between the ADC_{mean} or ADC_{min} vales and PET metabolic feature ($p > 0.5$).

Radiomic Features of Primary Tumors in Two Groups of Local and Metastatic CCA

As shown in Table 1, patients were classified into two major groups: (1) local disease, without nodal or metastatic spread of the tumor (N0M0, $n = 7$); (2) metastatic disease, with nodal

Table 4. Pearson correlation coefficients and associated p values between selected [^{18}F]FDG PET/MRI and ADC-derived radiomic features in primary cervical cancer

PET feature	ADC feature	Pearson correlation (ρ)	p value
Volume	Volume	0.8	<0.01
SUV _{mean}	ADC _{sphericity}	-0.7	<0.05
SUV _{max}	ADC _{sphericity}	-0.66	<0.05
SUV _{peak}	ADC _{sphericity}	-0.7	<0.05
MTV	ADC _{sphericity}	-0.54	<0.05
SUV _{peak}	ADC _{mean}	-0.35	0.22
Kurtosis	ADC _{mean}	-0.58	<0.05
MTV	ADC _{kurtosis}	0.59	<0.05
SUV _{peak}	ADC _{entropy}	-0.73	<0.05
MTV	ADC _{entropy}	-0.94	<0.01
TLG	ADC _{entropy}	-0.87	<0.01

Table 5. Significant difference was seen in 8 features between the two groups of patients with local and metastatic cervical cancer (these features include MTV, TLG, and entropy on PET/CT; MTV and TLG on PET/MRI; compactness and entropy on T2; and entropy on ADC images)

Imaging feature	AUC	95% CI	Cutoff value	p value
PET/MR _{MTV}	0.82	0.56–1.00	13.2	<0.05
PET/MR _{TLG}	0.85	0.64–1.00	64.5	<0.05
PET/CT _{MTV}	0.98	0.92–1.00	4.9	<0.05
PET/CT _{TLG}	0.92	0.75–1.00	23.17	<0.05
PET/CT _{entropy}	0.84	0.62–1.00	-2774	<0.05
ADC _{entropy}	0.86	0.6–1.00	-4,609,749	<0.05
T2 _{compactness}	0.86	0.62–1.00	35.35	<0.05
T2 _{entropy}	0.86	0.63–1.00	-10,496,043	<0.05

AUC area under the curve

and distant spread of the tumor (N1M1, $n=7$). Significant differences were seen in eight imaging features of primary tumors between the two groups of patients with local and metastatic CCa. These features include MTV, TLG, and entropy on PET from PET/CT; MTV and TLG on PET from PET/MRI; compactness and entropy on T2; and entropy on ADC images. The AUC and cutoff value for each of these imaging features are detailed in Table 5. Significantly strong correlation was noted among these eight factors ($\rho > 0.77$, $p < 0.001$) as shown on the correlation matrix (Fig. 2).

DISCUSSION

Our study demonstrated strong correlation among a large number of PET/CT, PET/MRI, CT, and MRI imaging features of the primary CCa. To the best of our knowledge, this is the first study in which the correlation of simultaneously acquired metabolic PET and morphologic CT and

morphologic and functional MRI intensity and advanced texture features are comprehensively investigated in primary CCa.

Integrated PET/MRI systems have provided a unique platform for simultaneous acquisition and analysis of the morphologic and functional imaging parameters for evaluation of the female pelvis [9, 22, 23]. Hybrid PET/MRI has the potential to provide more accurate co-registration of the images and reduce motion artifacts and acquisition time compared to sequentially acquired PET and MRI [10, 23]. Given the ionizing risk of radiation and lower soft tissue resolution of CT, PET/MRI is considered a superior and more favorable imaging modality for initial staging and sequential follow-up of several cancers, including pelvic cancers such as CCa [9, 23–25]. Multiple prior studies have shown the general feasibility of this new imaging technique, reproducibility of the results, and comparability of the SUVs derived from PET/CT and PET/MRI in various types of cancers including CCa [23, 26–28]. Our results showed a strong correlation between 219 out of 253 PET pairs of features on PET/CT and PET/MRI, which is in line with previously published studies.

Numerous previous publications have studied the role of PET/CT in diagnosis and staging of primary and recurrent cervical tumors [14, 29–31]. Strong correlation has been reported between the metabolic features on PET from PET/CT, with clinical and histopathological characteristics and prognosis of CCa including SCC [31–33]. Among all the parameters, SUV_{max} has been the most established and commonly applied parameter with strong association to the tumor biology including aggressiveness of the cancer and prediction of treatment response and clinical outcome [34, 35]. Our study demonstrated strong correlation between 110 out of 460 pairs of features on CT and PET from PET/CT, among which CT_{max} and CT_{compactness} showed the strongest positive correlation with PET metabolic features including SUV_{mean}, SUV_{max}, SUV_{peak}, TLG, and MTV. These results show that the higher tumor overall Hounsfield unit represented by CT_{max} (which could represent a combination of tumor solid component and enhancement) and higher tissue compactness is associated with higher tumor metabolism and [^{18}F]FDG uptake on PET. In addition, we found a strong inverse correlation between CT_{entropy} and PET uptake parameters showing that increased tumor heterogeneity is associated with lower SUVs and MTV in the tumors. Among the features of tumor heterogeneity, CT_{entropy} has been reported as one of the most reproducible features in many types of solid tumors [36]. However, application of the CT features without combination with PET or MRI is rare for evaluation of cervical tumors given the relatively lower soft tissue resolution of CT [9]. Recent efforts have been made to develop new CT-derived models and radiomic-based markers for prediction of nodal metastases [37]. Our results suggest that the advanced CT texture features might provide complementary information to these algorithms to improve cervical tumors stratification.

Radiomic features derived from MRI and simultaneous PET from PET/MRI have been proven to be helpful for tumor

characterization, monitoring treatment response, and prediction of survival in various types of cancers [38–40]. We found strong correlation between 102 out of 460 T2 and 63 out of 460 ADC pairs of features with PET from PET/MRI. There was a strong positive correlation between $T2_{\text{mean}}$ and SUV_{max} , SUV_{mean} and SUV_{peak} , $T2_{\text{compactness}}$ and SUV_{peak} , and between MTV and TLG on PET/MRI. These results suggest that the more compact tissue is associated with higher tumor metabolism. In addition, there was a strong inverse correlation between the $T2_{\text{sphericity}}$ and $T2_{\text{entropy}}$ with PET uptake values on PET/MRI suggesting that increased irregularity of tumor margins and decreased tumor heterogeneity are associated with increased [^{18}F]FDG uptake in primary CCa. Our results were in line with previous studies which showed the concordance of tumor volume measurements on T2 and PET from PET/MRI [41]. Although many previous studies have reported the role of T2 features on prediction of CCa local and distant invasion and survival [14, 29, 37, 42, 43], the correlation of T2 features with PET from PET/MRI has not been well established. To the best of our knowledge, this is the first study in which such correlation is being systematically investigated.

Results of studies on correlation of ADC values with PET features in CCa have been very heterogeneous. Interestingly, we found a strong correlation between the sphericity, entropy, and kurtosis on ADC with PET from PET/MRI metabolic features indicating the role of markers of tumor heterogeneity in further characterization of the primary CCa. These findings are in contrary with a study by Meyer et al. on 18 patients with cervical SCC which did not demonstrate a significant correlation between these characteristics on ADC and tumor metabolism on PET/MRI [44]. We detected no significant correlation between the ADC quantitative values such as ADC_{min} and ADC_{mean} , as markers of tumor cellularity, with PET from PET/MRI uptake measures. The majority of previous studies have demonstrated a strong correlation between ADC_{min} , ADC_{mean} , or their relative measures with local aggressiveness, nodal and distal metastasis, and risk of tumor recurrence in primary CCa [22, 23, 43, 44]. However, such correlation was not significant in CCa in some other recent studies [3, 29, 45–47]. Given that the majority of those studies have focused on the correlation of features on MRI and subsequently performed PET/CT, this discrepancy was previously suggested to be partly attributed to different attenuation correction fundamentals on PET/CT and time gap between the acquired PET and MRI images [23, 48]. However, more recent studies have shown confounding correlations between ADC and SUV values derived from simultaneous PET/MRI [22, 23, 44–47]. Other possibilities that could explain the discrepancy in these results is small sample size, different cervical tumor types and grades, differences in b values and DWI techniques, scanner field strength and geometry [49], and time of performed PET studies after [^{18}F]FDG administration [23]. Further evaluation of the ADC intensity and texture characteristics of CCa needs to be performed in larger cohorts.

It is crucial for the clinicians to identify the primary tumors with higher potential of local or distant metastases. In addition to the information on histopathological analyses of the primary tumors on initial workup, baseline imaging could help clinicians with providing information beyond solely the size and number of the lesions. Our results showed a significant difference in total of eight features between the local and metastatic primary cervical tumors. These features include MTV, TLG, and entropy on PET from PET/CT; MTV and TLG on PET from PET/MRI; entropy and compactness on T2; and entropy on ADC. Features of tumor metabolism such as SUV_{max} , MTV and TLG on PET/CT, ADC values, as well as skewness and kurtosis derived from first-order features have been most established as predictors of tumor nodal and lymph-vascular invasion in CCa [8, 50, 51]. By providing a cutoff value for the imaging features on the baseline scans of the newly diagnosed CCa, clinicians may be able to identify the more aggressive tumors with higher potential for metastasis and therefore modify the treatment strategy and attention on follow-up imaging. Larger studies with independent test sets are required in the future to further investigate the ability of PET/MRI features and their potential complementary and superior role to PET/CT for prediction of tumor nodal and distant metastases.

Although we analyzed a large number of radiomic features on multiple imaging modalities in primary CCa and demonstrated a significant correlation between a large number of imaging feature pairs, these results are considered preliminary and provide a basis for future clinical studies given the following limitations. The significant correlations reported on this study were not corrected for multiple comparisons given the very small sample size and significant compromise of potential correlations on this pilot study. Although some of the reported correlations may be present by chance, our exploratory analyses suggest the possible radiomic features that could be clinically impactful and further evaluated on studies with larger sample size. Given the small sample size, we did not include a detailed correlative analysis of various histological grades of CCa with radiomics. Our dataset did not include all of tumor stages and a correlation of imaging features with clinical follow-up and treatment response in patients was not performed. The second-order radiomic features such as Gray-level co-occurrence matrices (GLCM) metrics were not evaluated since direct clinical correlation has been difficult to be shown with these features [9]. Larger cohorts of patients with various types, grades, and stages of cervical tumors, and correlation with treatment response and survival are required to confirm and strengthen the results of this study.

In conclusion, our study presents the first comprehensive correlative analysis of multimodal PET/CT and PET/MRI of primary CCa. The results of this pilot study suggest the feasibility and potential use of hybrid PET/MRI radiomic features as non-invasive imaging biomarkers for characterization of primary cervical tumors prior to initiation of neoadjuvant treatment. The correlation of these features with tumor

biological properties and their potential role in prediction of metastasis are required to be further investigated in future larger prospective studies to help improve clinical care of patients with CCA.

Supplementary Information The online version contains supplementary material available at <https://doi.org/10.1007/s11307-021-01658-1>.

Author Contributions S.A.E., A.T.C., D.G., L.D., H.B., D.S., D.G., B.J.A., and O.A.C. contributed to the concept and design of the study. D.G., L.D., H.B., D.S., and O.A.C. contributed to the acquisition of the data. S.A.E., A.T.C., D.G., H.B., L.D., B.J.A., D.S., D.G., and O.A.C. contributed to the analysis and interpretation of the data. S.A.E., A.T.C., and O.A.C. drafted the manuscript. All authors read, critically revised, and approved the manuscript. All the authors agree to be accountable for all aspects of the work in ensuring that questions related to the accuracy or integrity of any part of the work are appropriately investigated and resolved.

Declarations

Ethics Approval The study has been approved by the institutional research ethics committee and have been performed in accordance with the ethical standards as laid down in the 1964 Declaration of Helsinki and its later amendments or comparable ethical standards.

Given its retrospective nature, the institutional ethical committee waived the need of written informed consent.

Conflict of Interest A.T.C. was partially supported by the Young Researchers R&D Project M2166 (MIMC3-PET/MR) financed by Community of Madrid and Rey Juan Carlos University. Other authors declare that they have no relevant disclosures.

References

- Bray F, Ferlay J, Soerjomataram I, Siegel RL, Torre LA, Jemal A (2018) Global cancer statistics 2018: GLOBOCAN estimates of incidence and mortality worldwide for 36 cancers in 185 countries. *CA Cancer J Clin* 68:394–424
- Papadia A, Gasparri ML, Genoud S, Bernd K, Mueller MD (2017) The combination of preoperative PET/CT and sentinel lymph node biopsy in the surgical management of early-stage cervical cancer. *J Cancer Res Clin Oncol* 143:2275–2281
- Yang Z, Xu W, Ma Y, Liu K, Li Y, Wang D (2016) (18)F-FDG PET/CT can correct the clinical stages and predict pathological parameters before operation in cervical cancer. *Eur J Radiol* 85:877–884
- Li K, Sun H, Lu Z et al (2018) Value of [(18)F]FDG PET radiomic features and VEGF expression in predicting pelvic lymphatic metastasis and their potential relationship in early-stage cervical squamous cell carcinoma. *Eur J Radiol* 106:160–166
- Nogami Y, Iida M, Banno K et al (2014) Application of FDG-PET in cervical cancer and endometrial cancer: utility and future prospects. *Anticancer Res* 34:585–592
- Zhou Z, Liu X, Hu K, Zhang F (2018) The clinical value of PET and PET/CT in the diagnosis and management of suspected cervical cancer recurrence. *Nucl Med Commun* 39:97–102
- Schick U, Lucia F, Dissaux G et al (2019) MRI-derived radiomics: methodology and clinical applications in the field of pelvic oncology. *Br J Radiol* 92:20190105
- Floberg JM, Fowler KJ, Fuser D et al (2018) Spatial relationship of 2-deoxy-2-[(18)F]-fluoro-D-glucose positron emission tomography and magnetic resonance diffusion imaging metrics in cervical cancer. *EJNMMI Res* 8:52
- Amorim BJ, Torrado-Carvajal A, Esfahani SA et al (2020) PET/MRI radiomics in rectal cancer: a pilot study on the correlation between PET- and MRI-derived image features with a clinical interpretation. *Mol Imaging Biol* 22:1438–1445
- Brendle CB, Schmidt H, Fleischer S, Braeuning UH, Pfannenber CA, Schwenzer NF (2013) Simultaneously acquired MR/PET images compared with sequential MR/PET and PET/CT: alignment quality. *Radiology* 268:190–199
- Atkinson W, Catana C, Abramson JS et al (2016) Hybrid FDG-PET/MR compared to FDG-PET/CT in adult lymphoma patients. *Abdom Radiol (NY)* 41:1338–1348
- Lambin P, Rios-Velazquez E, Leijenaar R et al (2012) Radiomics: extracting more information from medical images using advanced feature analysis. *Eur J Cancer* 48:441–446
- Gillies RJ, Kinahan PE, Hricak H (2016) Radiomics: images are more than pictures, they are data. *Radiology* 278:563–577
- Lucia F, Visvikis D, Desseroit MC et al (2018) Prediction of outcome using pretreatment (18)F-FDG PET/CT and MRI radiomics in locally advanced cervical cancer treated with chemoradiotherapy. *Eur J Nucl Med Mol Imaging* 45:768–786
- Catalano OA, Horn GL, Signore A et al (2017) PET/MR in invasive ductal breast cancer: correlation between imaging markers and histological phenotype. *Br J Cancer* 116:893–902
- Lucia F, Visvikis D, Vallieres M et al (2019) External validation of a combined PET and MRI radiomics model for prediction of recurrence in cervical cancer patients treated with chemoradiotherapy. *Eur J Nucl Med Mol Imaging* 46:864–877
- Amorim BJ, Hong TS, Blaszkowsky LS et al (2019) Clinical impact of PET/MR in treated colorectal cancer patients. *Eur J Nucl Med Mol Imaging* 46:2260–2269
- Catalano OA, Lee SI, Parente C, et al. (2021) Improving staging of rectal cancer in the pelvis: the role of PET/MRI. *Eur J Nucl Med Mol Imaging* 48:1235–1245. <https://doi.org/10.1007/s00259-020-05036-x>
- Esfahani SA, Heidari P, Halpern EF, Hochberg EP, Palmer EL, Mahmood U (2013) Baseline total lesion glycolysis measured with (18)F-FDG PET/CT as a predictor of progression-free survival in diffuse large B-cell lymphoma: a pilot study. *Am J Nucl Med Mol Imaging* 3:272–281
- Bhatla N, Berek JS, Cuello Fredes M et al (2019) Revised FIGO staging for carcinoma of the cervix uteri. *Int J Gynaecol Obstet* 145:129–135
- Koh WJ, Abu-Rustum NR, Bean S et al (2019) Cervical cancer, version 3.2019, NCCN Clinical Practice Guidelines in Oncology. *J Natl Compr Canc Netw* 17:64–84
- Brandmaier P, Purz S, Bremicker K et al (2015) Simultaneous [18F] FDG-PET/MRI: correlation of apparent diffusion coefficient (ADC) and standardized uptake value (SUV) in primary and recurrent cervical cancer. *PLoS One* 10:e0141684
- Grueneisen J, Beiderwellen K, Heusch P et al (2014) Correlation of standardized uptake value and apparent diffusion coefficient in integrated whole-body PET/MRI of primary and recurrent cervical cancer. *PLoS One* 9:e96751
- Catalano OA, Daye D, Signore A et al (2017) Staging performance of whole-body DWI, PET/CT and PET/MRI in invasive ductal carcinoma of the breast. *Int J Oncol* 51:281–288
- Pace L, Nicolai E, Aiello M, Catalano OA, Salvatore M (2013) Whole-body PET/MRI in oncology: current status and clinical applications. *Clin Transl Imaging* 1:31–44
- Beiderwellen K, Gomez B, Buchbender C et al (2013) Depiction and characterization of liver lesions in whole body [(1)(8)F]-FDG PET/MRI. *Eur J Radiol* 82:e669–675
- Rakheja R, Chandarana H, DeMello L et al (2013) Correlation between standardized uptake value and apparent diffusion coefficient of neoplastic lesions evaluated with whole-body simultaneous hybrid PET/MRI. *AJR Am J Roentgenol* 201:1115–1119
- Catalano OA, Coutinho AM, Sahani DV et al (2017) Colorectal cancer staging: comparison of whole-body PET/CT and PET/MR. *Abdom Radiol (NY)* 42:1141–1151
- Ho KC, Lin G, Wang JJ, Lai CH, Chang CJ, Yen TC (2009) Correlation of apparent diffusion coefficients measured by 3T diffusion-weighted MRI and SUV from FDG PET/CT in primary cervical cancer. *Eur J Nucl Med Mol Imaging* 36:200–208
- Chung HH, Kang SY, Ha S et al (2016) Prognostic value of preoperative intratumoral FDG uptake heterogeneity in early stage uterine cervical cancer. *J Gynecol Oncol* 27:e15
- Reuze S, Orhac F, Chargari C et al (2017) Prediction of cervical cancer recurrence using textural features extracted from 18F-FDG PET images acquired with different scanners. *Oncotarget* 8:43169–43179
- Cima S, Perrone AM, Castellucci P et al (2018) Prognostic impact of pretreatment fluorodeoxyglucose positron emission tomography/

- computed tomography SUVmax in patients with locally advanced cervical cancer. *Int J Gynecol Cancer* 28:575–580
33. Yagi S, Yahata T, Mabuchi Y et al (2016) Primary tumor SUVmax on preoperative FDG-PET/CT is a prognostic indicator in stage IA2–IIB cervical cancer patients treated with radical hysterectomy. *Mol Clin Oncol* 5:216–222
 34. Xue F, Lin LL, Dehdashti F, Miller TR, Siegel BA, Grigsby PW (2006) F-18 fluorodeoxyglucose uptake in primary cervical cancer as an indicator of prognosis after radiation therapy. *Gynecol Oncol* 101:147–151
 35. Antonsen SL, Loft A, Fisker R et al (2013) SUVmax of 18FDG PET/CT as a predictor of high-risk endometrial cancer patients. *Gynecol Oncol* 129:298–303
 36. van Rossum PSN, Xu C, Fried DV, Goense L, Court LE, Lin SH (2016) The emerging field of radiomics in esophageal cancer: current evidence and future potential. *Transl Cancer Res* 5:410–423
 37. Chen X, Liu W, Thai TC et al (2020) Developing a new radiomics-based CT image marker to detect lymph node metastasis among cervical cancer patients. *Comput Methods Programs Biomed* 197:105759
 38. Lohmann P, Kocher M, Ruge MI et al (2020) PET/MRI radiomics in patients with brain metastases. *Front Neurol* 11:1
 39. Weber M, Kessler L, Schaarschmidt B et al (2020) Treatment-related changes in neuroendocrine tumors as assessed by textural features derived from (68)Ga-DOTATOC PET/MRI with simultaneous acquisition of apparent diffusion coefficient. *BMC Cancer* 20:326
 40. Shaikh F, Dupont-Roettger D, Dehmeshki J, Kubassova O, Quraishi MI (2020) Advanced imaging of biochemical recurrent prostate cancer with PET, MRI, and radiomics. *Front Oncol* 10:1359
 41. Lai AYT, Perucho JAU, Xu X, Hui ES, Lee EYP (2017) Concordance of FDG PET/CT metabolic tumour volume versus DW-MRI functional tumour volume with T2-weighted anatomical tumour volume in cervical cancer. *BMC Cancer* 17:825
 42. Wu Q, Shi D, Dou S et al (2019) Radiomics analysis of multiparametric MRI evaluates the pathological features of cervical squamous cell carcinoma. *J Magn Reson Imaging* 49:1141–1148
 43. Ai Y, Zhu H, Xie C, Jin X (2020) Radiomics in cervical cancer: current applications and future potential. *Crit Rev Oncol Hematol* 152:102985
 44. Meyer HJ, Purz S, Sabri O, Surov A (2018) Cervical cancer: associations between metabolic parameters and whole lesion histogram analysis derived from simultaneous (18)F-FDG-PET/MRI. *Contrast Media Mol Imaging* 2018:5063285
 45. Sun H, Xin J, Zhang S et al (2014) Anatomical and functional volume concordance between FDG PET, and T2 and diffusion-weighted MRI for cervical cancer: a hybrid PET/MR study. *Eur J Nucl Med Mol Imaging* 41:898–905
 46. Pinker K, Andrzejewski P, Baltzer P et al (2016) Multiparametric [18F] fluorodeoxyglucose/[18F]fluoromisonidazole positron emission tomography/magnetic resonance imaging of locally advanced cervical cancer for the non-invasive detection of tumor heterogeneity: a pilot study. *PLoS One* 11:e0155333
 47. Surov A, Meyer HJ, Schob S et al (2017) Parameters of simultaneous 18F-FDG-PET/MRI predict tumor stage and several histopathological features in uterine cervical cancer. *Oncotarget* 8:28285–28296
 48. Martinez-Moller A, Souvatzoglou M, Delso G et al (2009) Tissue classification as a potential approach for attenuation correction in whole-body PET/MRI: evaluation with PET/CT data. *J Nucl Med* 50:520–526
 49. Rao RK, Riffel P, Meyer M et al (2012) Implementation of dual-source RF excitation in 3 T MR-scanners allows for nearly identical ADC values compared to 1.5 T MR scanners in the abdomen. *PLoS One* 7:e32613
 50. Zhao Q, Feng Y, Mao X, Qie M (2013) Prognostic value of fluorine-18-fluorodeoxyglucose positron emission tomography or PET-computed tomography in cervical cancer: a meta-analysis. *Int J Gynecol Cancer* 23:1184–1190
 51. Kidd EA, El Naqa I, Siegel BA, Dehdashti F, Grigsby PW (2012) FDG-PET-based prognostic nomograms for locally advanced cervical cancer. *Gynecol Oncol* 127:136–140

Publisher's Note Springer Nature remains neutral with regard to jurisdictional claims in published maps and institutional affiliations.